PROGRESS WITH ROTATIONAL PRINTING FOR THE FRONT SIDE METALLIZATION OF SILICON SOLAR CELLS

A. Lorenz[1], C. Gredy[1], M. Lehner[2], H. Brocker[3], J. Rohde[4], A. Senne[5], T. Strauch[1], H. Reinecke[6], F. Clement[1]

[1]Fraunhofer Institute for Solar Energy Systems (ISE), Heidenhofstr. 2, 79110 Freiburg, Germany
[2]Lehner Engineering GmbH, Ebnetstrasse 18, 9032 Engelburg, Switzerland
[3]Gallus Ferd. Rüesch AG, Harzbüchelstrasse 34, 9016 St. Gallen, Switzerland
[4]Zecher GmbH, Görlitzer Str.2, 33098 Paderborn, Germany
[5]ContiTech Elastomer-Beschichtungen GmbH, Breslauer Str. 14, 7154 Northeim, Germany
[6]Albert-Ludwigs-Universität, Institut für Mikrosystemtechnik, Georges-Köhler-Allee 101, 79110 Freiburg, Germany

ABSTRACT: The current cost pressure within the photovoltaic industry requires innovative approaches to increase productivity and reduce production costs. The use of highly productive rotational printing methods offers the potential to increase the throughput of the cost-intensive metallization process by the factor 2 to 3. Within this work, we present two innovative rotational printing technologies – flexographic printing and rotary screen printing – for the front side metallization of Silicon solar cells. We show that both technologies can realize contact fingers with a lateral finger resistance R_L below 10 Ω/cm in one printing step which is sufficient for busbarless solar cells with multi-wire interconnection. For flexographic printing, we found a strong impact of the anilox roller properties on geometry and lateral resistance of the contact fingers. A finger resistance of R_L = 8.5 Ω/cm which is sufficient for wire-interconnected busbarless solar cells could be achieved using an anilox roller with a very large dip volume of V_D = 16.5 cm³/cm². For rotary screen printing, a considerable increase of the finger width due to spreading of the Ag-paste proved to be the major challenge for further development.
Keywords: Silicon Solar Cells, Manufacturing and Processing, Metallization, Rotation Printing

1 INTRODUCTION

1.1 Rotational printing technology for solar cells

Though competition and high cost pressure in the industrial fabrication of crystalline Silicon (Si) solar cells demands new approaches to decrease costs and increase productivity. Considering the fabrication process of solar cells, front and rear side metallization is a particularly cost-intensive production step. To date, flatbed screen printing (FSP) is still the predominant metallization technique for crystalline Si solar cells and will also play an important role in the future. However, new technological approaches can help to increase throughput of metallization lines considerably. Such a promising approach are rotational printing technologies which are investigated by Fraunhofer ISE since 2011 [1]. Rotational printing methods are in contrast to various other technological approaches well established and used for a wide range of industrial applications. These printing methods can realize a very high printing speed of up to 800 m/min. on web-based materials [2]. Such a high throughput is obviously not possible for solar cell metallization lines due to the necessity of a precise delivery and alignment of the Si wafers. Yet, using rotational printing methods will enable a considerable increase in throughput by the factor 2 to 3 compared to current standard metallization lines. However, a metallization line using rotational printing must be able to meet the challenging requirements of solar cell front and rear side metallization, namely ultra-fine contact fingers with sufficient lateral conductivity on the front side and a homogeneous Aluminium (Al) layer on the rear side. Within this work, two rotational printing methods for the front and rear side metallization of Si solar cells are presented. Recent achievements with both technologies are shown and the path to an industrial application is discussed.

1.2 Flexographic printing technology

Flexographic printing is a widely used rotational printing method, mainly in package printing on roll-to-roll materials like cardboard, paper or foil. A low-cost flexible relief printing plate is used as image carrier (Figure 1). Compressible foam tape is applied below the printing plate to support a homogeneous ink transfer. The low-viscous silver ink is transferred from the ink chamber onto the so-called anilox roll, a steel cylinder with finely engraved micro-wells on a chromium or ceramic surface. The amount and geometry of the micro-wells defines the amount of transferred ink and is known as dip volume V_D [cm³/m²]. The screen count of the micro-wells can vary between 100 and 700 lines/cm and the (nominal) dip volume between 16.5 and 1.0 cm³/m². Excessive ink is removed by a doctor blade before the anilox roller wets the elevated areas of the printing plate with a uniform layer thickness. The elevated areas of the printing plate are directly printed onto the substrate. The flexible printing plate and the relatively low printing pressure allow a homogeneous and precise printing even on very rough substrates like textured silicon wafers.
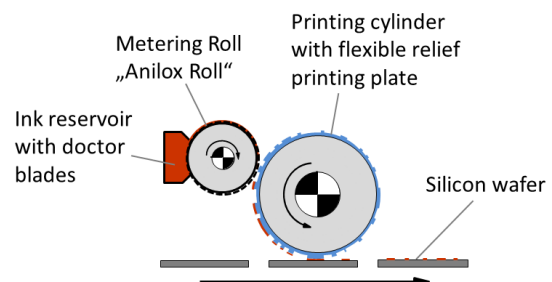

Figure 1: Schematic of a flexo printing unit for solar cell metallization

Flexographic printing is able to realize a front side grid of busbarless solar cells for multi-wire interconnection with less than 5 mg of silver [3]. Previous work [4,5] demonstrated a mean contact finger width of 23 μm on silicon solar cells in a single printing step. However, the challenge is to realize a good lateral conductivity of the front side grid. Thus, flexographic printing is particularly well-suited for innovative solar cell concepts which do not necessarily need a low lateral finger resistance like Meyer Burger's SmartWire Connection Technology (SWCT) [6].

1.3 Rotary screen printing technology

Rotary screen printing (RSP) is able to combine the technological advantages of screen printing thick film metallization with the potential high throughput of rotational printing. To date, this technology is primarily used for web-based materials like labels or textiles [7] and can realize a printing speed of up to 100 m/min. First attempts to use this technology for solar cell metallization date back to the year 1999 [8]. However, to the best knowledge of the authors, no results on Si solar cells have been published so far.

Similar to flatbed screen printing, a woven screen mesh covered with a partly open emulsion layer is used as printing form. However, in contrary to the flat printing form of FSP, cylinder-shaped screens are used for RSP. The meshes of such screens consist of up to 400 threads per inch (mesh count). However, the thickness of the threads needs to be greater (minimum 25 to 30 μm) than the threads of a flatbed screen to ensure an adequate stability of the screen cylinder. Using FSP, the paste is pressed through the openings of the flat screen using a flood bar in a first step and a flexible squeegee in a second step. In contrary, RSP uses a fixed squeegee within a constantly rotating screen cylinder to transfer the paste through the openings of the screen (Figure 2). To ensure a good ink transfer, a lower paste viscosity compared to flatbed screen printing pastes is required. Due to the higher amount of applied paste, RSP is an interesting alternative for the rear side metallization and the front side metallization of Si solar cells.
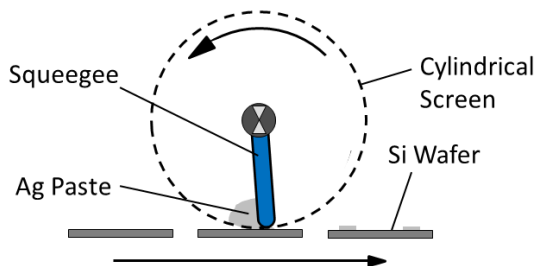

Figure 2: Schematic of a rotary screen printing unit for solar cell metallization.

1.4 Aim of the Experiment

A modern industrial FSP metallization line is able to print contact fingers with an average width of 45-55 μm and a lateral resistance of 0.3 to 0.5 Ω/cm [9]. While a narrow finger width is favorable to reduce j_{sc}-losses, lateral finger resistance depends on the concept for solar cell interconnection. Traditional H-pattern solar cells with 3 busbars require a lateral finger resistance of 0.3 to 0.5 Ω/cm to ensure a small series resistance contribution of the grid. Thus, flatbed screen printing is still the most suitable metallization method for such solar cells. However, next generation solar cells with 5 printed busbars or wire-interconnected busbarless solar cells require a considerably lower lateral resistance. R_L should not exceed 1.5 Ω/cm for 5-busbar cells and 10 Ω/cm for busbarless solar cells interconnected with 18 wires by SWCT [6]. It is the aim of this experiment to evaluate the current opportunities of flexographic printing and rotary screen printing with respect to solar cell front side metallization. It will be clarified whether both technologies are able to meet the challenging demands regarding finger width and lateral finger resistance.

2 EXPERIMENTAL SETUP

2.1 Feasibility study for flexographic printing

Industrially pre-produced Czrochalski-grown p-type Si (Cz-Si) precursors with 156 mm edge length are used for the test. The precursors have an n-type emitter with a sheet resistance of $R_{sh} \approx$ 85-90 Ω/sq. and a SiNx anti-reflection coating (ARC) on the front side. A roll-to-flat flexographic printing platform Nissha Angstromer S15 is used to apply the front side metallization of the solar cells. This machine has a vacuum substrate holder to fix the wafer during the printing process. The position of the vacuum substrate holder perpendicular to the axis of the printing cylinder (z-position) is adjusted by a micrometer spindle. Each wafer is positioned manually on the vacuum table. Printing speed is kept constant at $v_p \approx$ 300 mm/s during the experiment. The optimum printing pressure (= minimal pressure which is required to print the whole printing image without missing areas) is determined by stepwise adjustment of the vacuum substrate holder in z-direction. The identified optimum printing pressure is further kept constant during the printing process. All wafers are dried in a cabinet drier at T = 200°C for 2-5 minutes directly after printing. Subsequently, all wafers with test pattern are contact fired using a fast firing furnace with a peak set temperature of $T_{FFO} = 830$°C.

A ceramic band anilox roller with 3 differently engraved sections is fabricated for the experiment. Each section has a different screening and dip volume V_D (see Table 1).

Table 1: Parameters of the band anilox roller

	Well Geometry	Screening [l/cm]	Dip Volume V_D [cm³/m²]
Band 1	Hexagonal	700	16.5
Band 2	Hexagonal	340	6.3
Band 3	Hexagonal	100	1.0

A test layout with 3 identical sections (corresponding to the bands of the anilox roller) is fabricated using a *ContiTech Laserline* CSC flexographic printing plate. The test layout contains finger elements with nominal widths between 5 and 50 μm and measurement patterns for contact resistance measurement using transfer-length method (TLM) [10]. Thus, identical test patterns in each section on the printing plate can be printed with all 3 anilox bands in parallel (Figure 3).
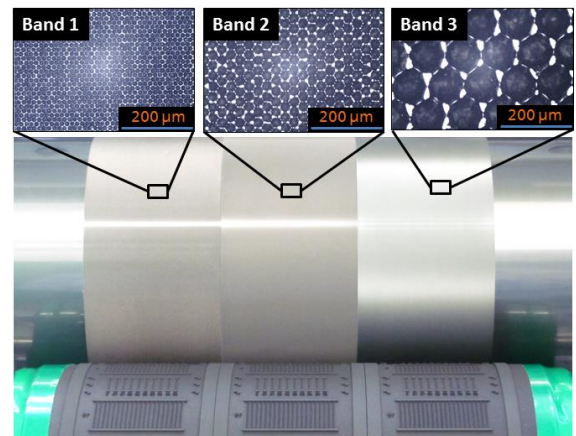

Figure 3: Microscopic images of the anilox roller with 3 differently engraved band sections

The silver ink is developed in-house and contains silver particles for metal-semiconductor contact formation, lead glass as a sintering additive, solvents, synthetic resin as binder and further additives to adjust viscosity, dispersion and electrical contact formation to the emitter. The formulation of the ink is based on a previously developed aerosol jet ink [11] and has been gradually optimized for flexographic printing in previous experiments [5,12,13].

2.2 Feasibility study for rotary screen printing

The feasibility study for rotary screen printing is carried out on a Gallus EM 280 label printing machine (Figure 4). This machine is designed to print on continuous web materials like foil or paper web. A commercially available Ag-paste for solar cell front side metallization is diluted iteratively to an adequate viscosity for rotary screen printing. To enable a transport of the wafers through the rotary screen printing unit, every wafer is fixed individually on the foil web before each print run. Printing speed is set to $v_p \approx 170$ mm/s. A test layout comprising contact finger elements with a nominal width between 20 and 55 µm is printed on multicrystalline Si wafers (mc-Si) with SiN$_x$-ARC.
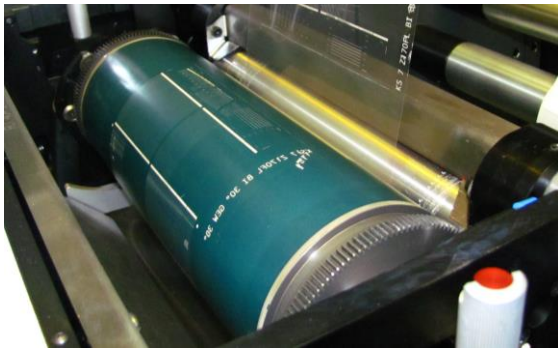

Figure 4: Rotational screen printing unit of the Gallus EM 280 label printing machine.

2.3 Characterization of contact finger geometry

The three-dimensional geometry (width w_f, height h_f, cross-section area A_f) of the contact fingers is measured using an *Olympus Lext* confocal microscope (amplification factor 500x). On the flexo-printed test patterns, 10 fingers are measured within each of the three anilox band sections resulting in 30 measurements per wafer and approx. 210 measurements in total. On the wafers printed with rotary screen printing, 7 fingers per wafer are measured on four wafers, resulting in 28 measurements in total. To ensure an objective and reproducible analysis of the finger geometry, all microscopic images are analyzed using the image analysis algorithm FineUp 1.4 which has been developed at Fraunhofer ISE [14]. This algorithm enables a precise and reproductive quantification of all relevant contact finger geometry parameters.

2.4 Electrical characterization of contact fingers

Using four-point measurement method, absolute finger resistance R_f is measured on the same contact fingers which have been previously analyzed regarding finger geometry. Subsequently, lateral finger resistance per unit length R_L [Ω/cm] is calculated with the known distance of the measurement pins.

3 RESULTS AND DISCUSSION

3.1 Flexo-printed contact fingers

Figure 5 shows the relation of nominal finger width w_n in the test layout and the flexo-printed finger width w_f. The results show with good approximation a linear relation between both parameters.
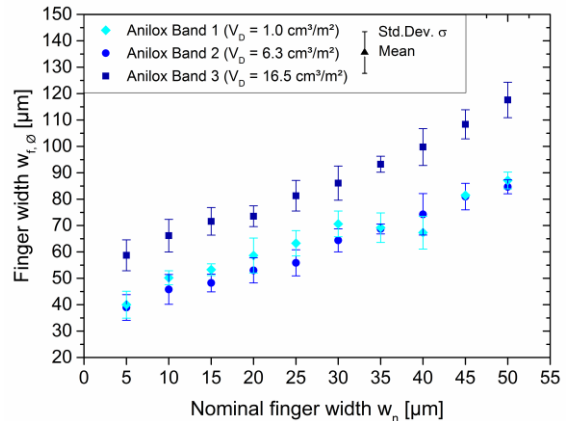

Figure 5: Printed finger width w_f depending on the anilox band section and nominal finger width w_n

All contact fingers reveal a considerable finger width increase in comparison to the nominal width w_n. This increase primarily originates from deformation effects of the compressed elevated fine line elements on the printing plate during the printing process. Bould et al. [15] deeply investigated these effects which they classified as *(flank) barreling*, *(surface) extension* and *ink spreading* (Figure 6).
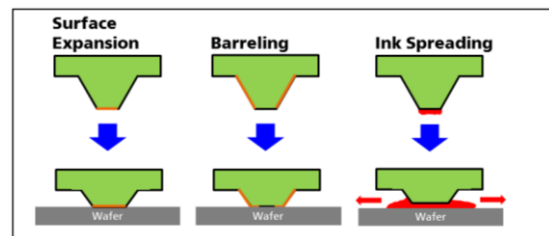

Figure 6: Schematic of plate deformation effects and ink spreading phenomena of the fine line elements on the printing plate under pressure (modified illustration based on [15]).

Particularly barreling and surface extension effects are strongly related to the mechanical stability of the finger elements. Broad finger elements are relatively stable against deformation. Thus, fingers with a nominal width of $w_n = 50$ µm only show a moderate gain (percentage increase of w_f compared to w_n) between 170 to 240 % after printing. Narrow finger elements are less stable and thus suffer from a considerably stronger gain between 780 and 1180 % (for $w_n = 5$ µm). However, narrowest fingers can be realized with a small nominal finger width. These findings correspond to the results of earlier studies [13] and underline the necessity to minimize the width and increase the stability of the finger elements on the plate in order to print narrow contact fingers. A path to address this challenge is an optimization of the three-dimensional finger geometry on the plate which can be realized using the laser ablation process [16]. The results furthermore reveal a considerable influence of the anilox dip volume on the finger width. Usually, a

great line screening should be beneficial for a precise printing of fine lines. Thus, one would expect smaller fingers within band section 1 (l = 700 l/cm) compared to band section 2 (l = 340 l/cm) and 3 (l = 100 l/cm). However, band 1 and 2 reveal closely comparable results regarding finger width w_f. This indicates that the deformation of the fine line elements on the plate together with ink spreading effects are primarily responsible for the printed finger width w_f rather than the screening of the anilox roller. Band 3 shows a stronger gain of finger width compared to band 1 and 2. As the dip volume V_D and thus the amount of transferred ink of this band is considerably higher, finger elements on the plate are covered with much more ink when contacting the anilox roller. Thus, the impact of ink spreading might be considerably higher which could be responsible for the broader contact fingers. Figure 7 shows the relation between w_n and mean finger cross-section area A_f of the printed contact fingers. A_f is primarily influenced by the dip volume V_D of the anilox roll as more ink is transferred onto the fine line finger elements and thus on the wafer surface. Yet, the measurement data and a visual inspection of the microscopic images of the contact fingers revealed that only band section 3 is capable to transfer a noteworthy amount of ink. Fingers printed with this band have a finger height of $h_f \approx 6$-7 µm, fingers printed with band 1 and 2 a considerably lower and strongly varying height of $h_f \approx 0.5$ to 3 µm. While the cross-section area A_f of fingers printed with band 3 is relatively uniform and increases linearly with w_n, it is very low and does not increase with w_n for band 1 and 2.
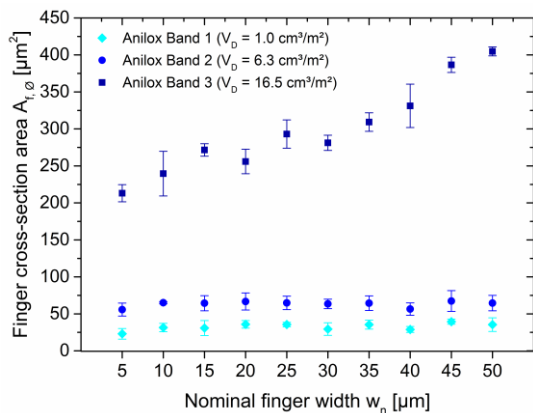

Figure 7: Mean finger cross-section area A_f depending on anilox band section and nominal finger width w_n
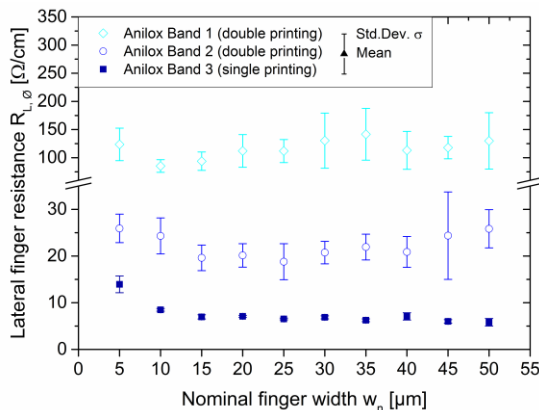

Figure 8: Lateral finger resistance R_L depending on anilox band section and nominal finger width w_n

Figure 8 illustrates the measured mean lateral finger resistance R_L depending on the anilox band section and the nominal finger width w_n. It is clearly visible that R_L is strongly influenced by the dip volume of the anilox band section. Fingers printed with band sections 1 and 2 did not obtain meaningful R_L-values in a single printing step. Thus, Figure shows the R_L-results of double printed fingers for these two band sections. Yet, fingers in band 1 obtained very high R_L-values even after applying a double printing step. R_L-values of (double printed) fingers in band 2 are considerably lower, yet still by the factor 2-3 too high for the front side metallization of multi-wire solar cells. However, fingers printed with band 1 obtained very promising R_L-values between 5.8 Ω/cm ($w_n = 50$ µm) and 13.9 Ω/cm ($w_n = 5$ µm) in a single printing step. The lateral resistance of the fingers in this band section decreases moderately with increasing nominal finger width and remains relatively stable for $w_n \geq 15$ µm. Summarizing the results it can be stated that only anilox band section 3 with a large dip volume is capable to realize fingers with sufficiently low R_L-values in a single printing step. The target of fingers with $R_L \leq 10$ Ω/cm for wire-interconnected busbarless solar cells can thus be realized using flexographic printing with a large anilox roller dip volume.

To assess the grid-related *FF*-loss of a flexo-printed front side grid, the theoretic contribution of lateral finger resistance R_L to the series resistance $r_{s,grid}$ and the resulting *FF*-loss ΔFF_{grid} of a virtual solar cell with SWCT interconnection is calculated using models based on [17–19]. The calculation assumes that all fingers of the front side grid are printed homogeneously and thus would achieve the same geometric and electric results. A flexo-printed busbarless front side grid with 100 contact fingers and wire-interconnection using 18 wires is assumed. The achieved results (R_L and w_f) of the flexo printed contact fingers are taken as input parameter. Losses due to transition resistance between contact fingers and wires are neglected. The results are shown in Table 2.

Table 2: Calculated series resistance $r_{s,grid}$ contribution and fill factor loss ΔFF_{grid} of a virtual flexo-printed solar cell with SmartWire-interconnection (18 wires)

	R_L [Ω/cm]	$r_{s,grid}$ [Ω/cm²]	ΔFF_{grid}
Band 1*	85.3	7.95	-45.31
Band 2*	24.3	0.23	-1.29
Band 3**	8.5	0.08	-0.45
*double printing step		**single printing step	

The results of the calculations again underline the necessity to use an anilox roll with a large dip volume V_D. Using an anilox roller with a smaller dip volume like band 1 and 2 leads to unacceptably high R_L-values and thus induces considerable *FF*-losses even when applying a double printing step.

To evaluate the shading impact of the printed front side grid, the theoretic j_{sc}-loss is calculated with known photo-generated current j_{ph} and total percentage of shading on the front side $A_{sh\%}$ (caused by the printed front side grid and the wires). The calculation is carried out for an assumed SWCT interconnection with 18 wires (wire diameter $d_{wire} = 200$ µm). An effective shading width of 75 % is assumed for the round wires [6]. A photo-generated current density of $j_{ph} = 40.9$ mA/cm² is taken as basis. Reflection and absorption effects due to module encapsulation on j_{sc} are not considered. It is furthermore

assumed that the flexo-printed front side grid is printed homogeneously with the same finger width on the whole wafer. The calculated theoretical j_{sc}-loss for a grid printed with band 1, 2 and 3 is shown in Table 3.

Table 3: Calculated total shading percentage and resulting j_{sc}-loss for a virtual wire-interconnected solar cell with flexo-printed front side grid using anilox band 1 to 3

	w_f [µm]	$A_{sh\%}$ [%]	Δj_{sc} [mA/cm²]
Band 1*	50	5.3	-2.2
Band 2*	46	5.1	-2.1
Band 3**	66	6.3	-2.6
*double printing step		**single printing step	

As expected, the broader finger width of anilox band section 3 leads to an increased j_{sc}-loss due to increased shading. Considering the fact that suitable contact fingers can only be printed with band 3 it must be the main focus of further development to decrease the finger width. A possible path to achieve this goal is an optimization of the ink rheology to prevent excessive spreading.

3.2 Rotary screen-printed contact fingers

Figure 9 shows the printed mean finger width w_f of rotary screen-printed contact fingers in relation to the opening of the fingers in the screen (further referred to as nominal width w_n). A visual inspection of the fingers revealed uninterrupted contact fingers down to a nominal finger width of $w_n = 30$ µm. The smallest mean finger width which could be achieved was $w_f = 68$ µm (printed with $w_n = 30$ µm). Fingers printed with a screen opening of $w_n = 25$ µm suffered from multiple interruptions and could not be printed stable.
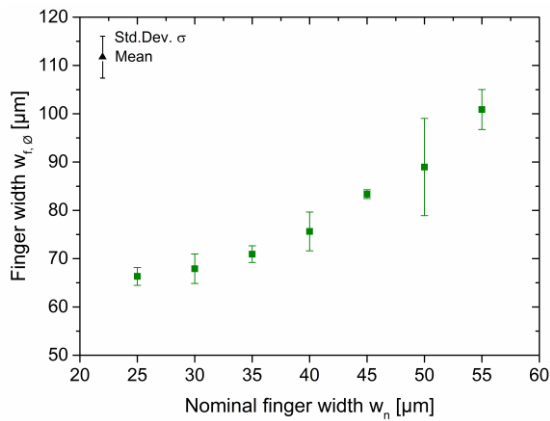

Figure 9: Relation between nominal finger width w_n in the test layout and printed finger width w_f using rotational screen printing

The rotary screen-printed finger width is about 1.7 to 2 times broader than fingers printed with flatbed screen printing at the same screen opening. The origin of this gain is primarily related to a stronger spreading of the diluted Ag-paste. A good measure for the spreading tendency of a screen printing paste is the yield stress τ_y [20]. The yield stress is determined using an algorithm developed by Pospischil et al. at Fraunhofer ISE [21]. Figure 10 shows the yield point of a commercially available Ag-paste before and after dilution to an adequate viscosity for rotary screen printing. The yield stress τ_y of the diluted paste is considerably lower which indicates an increased spreading capability on the wafer surface directly

after printing. Optimizing the rheological properties of the Ag-paste must be the main route to obtain narrower contact fingers using rotary screen printing.
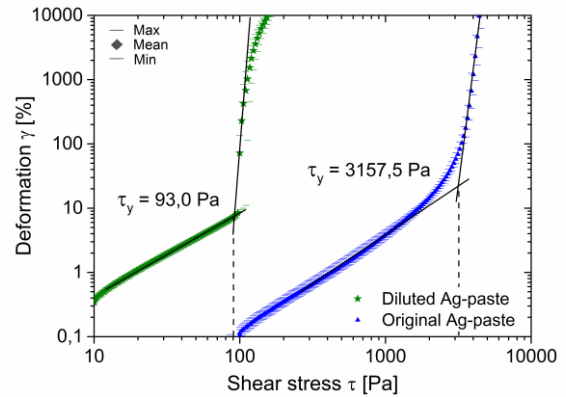

Figure 10: Yield stress τ_y of the diluted Ag-paste for rotary screen printing and the original non-diluted Ag-paste for flatbed screen printing.

Finger height h_f and cross-section area A_f increases linearly with w_n. This indicates that more paste can be transferred if it is pressed through a broader screen opening. Finger resistance R_L decreases as expected with increasing cross-section area (Figure 11). The very high R_L-values of fingers printed with $w_n = 25$ µm is most likely caused by multiple interruptions and constrictions. However, fingers printed with a screen opening of $w_n = 30$ µm or more could be printed without interruptions and obtained relatively low mean lateral resistances between $R_{L,max} = 3.6$ Ω/cm ($w_n = 30$ µm) and $R_{L,min} = 1.1$ Ω/cm ($w_n = 55$ µm).
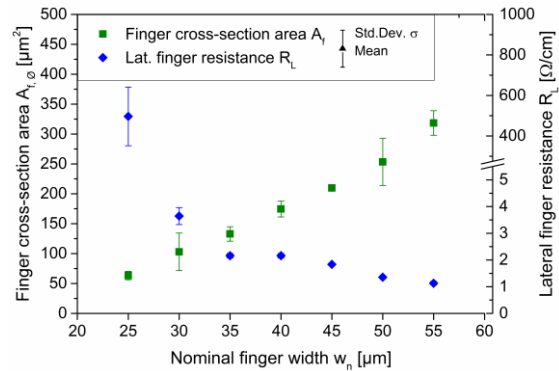

Figure 11: Finger cross-section area A_f and lateral finger resistance R_L depending on the nominal finger width w_n

Similar to the results for flexo printing, series resistance contribution $r_{s,grid}$ and fill factor loss ΔFF_{grid} of a virtual busbarless solar cell with wire-interconnection (18 wires) is calculated for three different nominal widths. Again, a front side grid with 100 homogeneously printed contact fingers is assumed. The further assumptions are similar to the previously described calculation in section 3.1. The results are shown in Table 4.

Table 4: Calculated series resistance contribution and fill factor loss of a virtual rotary screen-printed solar cell with SmartWire-interconnection (18 wires)

w_n	R_L [Ω/cm]	$r_{s,grid}$ [Ω/cm²]	ΔFF_{grid}
30	3.6	0.03	-0.19
45	1.8	0.02	-0.10
55	1.1	0.01	-0.06

The calculation shows that a front side grid printed with rotary screen printing does only give a negligible contribution to series resistance of the wire-interconnected solar cell.

Also, total percentage of shading on the front side $A_{sh\%}$ and the resulting j_{sc}-loss Δj_{sc} of grid and wires are calculated as described beforehand. The results are shown in Table 5.

Table 5: Calculated total shading percentage $A_{sh\%}$ and resulting j_{sc}-loss for a virtual wire-interconnected solar cell with rotary screen-printed front side grid and SmartWire-interconnection (18 wires)

w_n	w_f [μm]	$A_{sh\%}$ [%]	Δj_{sc} [mA/cm²]
30	68	6.4	-2.6
45	83	7.4	-3.0
55	101	8.5	-3.5

Shading losses are significant due to the relatively broad mean finger width w_f. Thus, further optimization in the field of rotary screen printing must focus on a considerable reduction of the printed finger width which could be achieved by a rheological optimization of the printing paste.

4 CONCLUSION

Within this work, we showed that both approaches – flexographic printing and rotational screen printing – are able to realize a suitable front side metallization for busbarless solar cells with wire interconnection.

With respect to flexographic printing it has been shown that the anilox roller has a considerable impact on the geometry and lateral resistance of the printed contact fingers. Using an anilox roller configuration with a very high dip volume of $V_D = 16.5$ cm³/m² led to contact fingers with a mean lateral resistance of $R_L = 8.5$ Ω/cm. Calculations of series resistance contribution and *FF*-loss revealed that a large dip volume is necessary to realize adequate contact fingers in a single print run. Using smaller dip volumes was beneficial for a narrow finger width. Yet the contact fingers showed very high R_L-values even after applying a double printing step. It was further shown that narrow printing lines on the printing plate are beneficial for narrow contact fingers despite of a stronger deformation under pressure. While the results are very promising with respect to an industrial application, further development is still required. Such attempts must focus on realizing narrower contact fingers with a comparably low R_L. The path to follow is a careful selection of the anilox roller specification, an optimization of the contact finger stability on the plate and a further optimization of the ink rheology.

The second experiment focused on rotary screen printing technology. It has been shown that uninterrupted contact fingers can be printed down to a nominal width of $w_n = 30$ μm. Commercially available Ag-paste can be used, yet the paste has to diluted to a lower viscosity. It was shown that the dilution strongly affects the yield point τ_0 of the paste and – in consequence – leads to an increased paste spreading. Thus, fingers printed with an opening of 30 μm obtained a significantly broader finger width of $w_f = 68$ μm. The fingers showed low mean lateral resistances between $R_{L,max} = 3.6$ and $R_{L,min} = 1.1$ Ω/cm. While the *FF*-loss of a theoretic rotary screen-printed grid should be negligible for a multi-wire interconnection, the relatively broad finger width w_f would induce a considerable j_{sc}-loss. Further optimization should thus focus on realizing narrower contact fingers by adjusting the rheological properties of the paste.

In summary, we successfully demonstrated the potential of two innovative rotational printing methods for the front side metallization of busbarless solar cells with multi-wire interconnection.

6 REFERENCES

[1] Frey M, Clement F, Dilfer S, Erath D, Biro D. Front-side Metallization By Means Of Flexographic Printing. *Energy Procedia* 8, 2011, p. 581–586.

[2] Windmöller & Hölscher. Technical Data Sheet Vistaflex C. Available at: http://www.wuhlengerich.de/de/printing/druckmaschinen/flexodruckmaschinen/vistaflex-c/; 2015 [accessed 09.01.2015].

[3] Lorenz A, Gredy C, Senne A, Beyer S, Yao Y, Papet P, Ufheil J, Reinecke H,Clement F. Rotational Printing Technology for the Metallization of Highly Efficient Busbarless Solar Cells [Submitted for publication 2016].

[4] Thibert S, Jourdan J, Bechevet B, Mialon S, Chaussy D, Reverdy-Bruas N, Beneventi D. Study of the high throughput flexographic process for silicon solar cell metallisation. *Progress in Photovoltaics* 2015.

[5] Lorenz A, Kalio A, Hofmeister GT, Nold S, Kraft A, Bartsch J, Wolf A, Dreher M, Clement F, Biro D. Flexographic Printing – High Throughput Technology for Fine Line Seed Layer Printing on Silicon Solar Cells. *Proc. of the 28th EUPVSEC* 2013, p. 1017–1023.

[6] Söderström T, Papet P, Yao Y, Ufheil J. SmartWire Connection Technology; 2014.

[7] Gallus Ferd. Rüesch AG. Gallus Screeny – Innovativer Siebdruck. Available at: http://www.gallusgroup.com/de/DesktopDefault.aspx/tabid-397/600_read-2147; 2014 [accessed 27.03.2015].

[8] Hahne P. Innovative Druck- und Metallisierungsverfahren für die Solarzellentechnologie. PhD Thesis, Fernuniversität Hagen, 2000.

[9] ITRPV. International Technology Roadmap for Photovoltaic: 2015 results. 7th ed; 2016.

[10] Kontermann S, Hörteis M, Ruf A, Feo S, Preu R. Spatially resolved contact-resistance measurements on crystalline silicon solar cells. *Phys. Status Solidi (a)* 2009, doi:10.1002/pssa.200925077.

[11] Hörteis M, Mette A, Richter P, Fidorra F, Glunz S. Further progress in metal aerosol jet printing for front side metallization of silicon solar cells. *Proc. of the 22nd EUPVSEC* 2007, p. 1039–1042.

[12] Lorenz A, Kalio A, Barnes Hofmeister T, Kraft A, Bartsch J, Clement F, Reinecke H, Biro D. Developing a high throughput printing technology for silicon solar cell front side metallisation using flexography. *J. Print Media Technol. Res.* 4, 2014, p. 227–240, doi:10.14622/JPMTR-1408.

[13] Lorenz A, Senne A, Rohde J, Kroh S, Wittenberg M, Krüger K, Clement F, Biro D. Evaluation of Flexographic Printing Technology for Multi-busbar Solar Cells. *Energy Procedia* 67, 2015, p. 126–137, doi:10.1016/j.egypro.2015.03.296.

[14] Strauch T, Demant M, Lorenz A, Haunschild J, Rein S. Two Image Processing Tools to Analyse Alkaline Texture and Finger Geometry in Microscope Images. *Proc. of the 29th EUPVSEC* 2014.

[15] Bould DC, Claypole TC, Bohan MFJ. An investigation into plate deformation in flexographic printing. *Proceedings of the Institution of Mechanical Engineers, Part B: Journal of Engineering Manufacture* 218, 2004, p.1499–1511

[16] A. Lorenz, C. Gredy, A. Senne, S. Beyer, Y. Yao, P. Papet, J. Ufheil, H. Reinecke, F. Clement. Flexoprinted busbarless solar cells for multi-wire interconnection. To be published in Energy Procedia 2016.

[17] Fellmeth T, Clement F, Biro D. Analytical Modeling of Industrial-Related Silicon Solar Cells. *IEEE J. Photovoltaics* 4, 2014, p. 504–513, doi:10.1109/JPHOTOV.2013.2281105.

[18] Fellmeth T. Silicon Solar Cells for the Application in Low Concentrator Systems-Development and Characterization. PhD Thesis, Eberhard Karls Universität, Tübingen, 2014.

[19] Mette A. New concepts for front side metallization of industrial silicon solar cells. PhD Thesis, Albert-Ludwigs-Universität, Freiburg, 2007.

[20] Mezger TG. Das Rheologie-Handbuch: Für Anwender von Rotations- und Oszillations-Rheometern. Farbe und Lack Edition. 4th ed. Hannover: Vincentz Network; 2012.

[21] Pospischil M, Specht J, Konig M, Horteis M, Mohr C, Clement F, Biro D. Paste Rheology Correlating With Dispensed Finger Geometry. *IEEE J. Photovoltaics* 4, 2014, pp. 498–503, doi:10.1109/JPHOTOV.2013.2278657.